ORIGINAL PAPER

Kinetics, isotherms and thermodynamics: iodine ion adsorption on Ag$_2$O–titanate nanostructures

T. Mostatabi[1] · A. H. Hassani[2] · S. Janitabar Darzi[3] · A. Nilchib[3]

Abstract

Silver oxide titanate nanotubes (Ag$_2$O@TNTs) and silver oxide titanate nanofibers (Ag$_2$O@TNFs) were synthesized by hydrothermal method with high alkalinity and used as adsorbents to remove iodine ions from aqueous solutions. The synthesized adsorbents, characterized by using X-ray Diffraction, Fourier Transform Infrared Spectroscopy, Scanning Electron Microscope, Transmission Electron Microscopy, and Brunauer–Emmett–Teller and Zeta-potential analysis. We evaluated iodine ion adsorption on Ag$_2$O@TNTs and Ag$_2$O@TNFs based on various factors like contact time, pH, initial concentration, adsorbent weight, and temperature through batch experiments. Our findings identified the optimal conditions for I$^-$ ion adsorption: pH 7, an initial concentration of 100 mg L^{-1}, 0.05 g of adsorbent per 20 ml, temperature $= 25 \pm 1$ °C, and about 30 min of contact time. The pseudo-second-order model best describes the adsorption kinetics, and the Langmuir model fits the adsorption isotherms more closely. The maximum uptake capacity of I$^-$ ions was found from the Langmuir model for I$^-$ ions was 344.83 (mg g^{-1}) and 277.77 (mg g^{-1}) at 298 K and removal rates of 83.4% and 78.8%, for Ag$_2$O@TNT and Ag$_2$O@TNF, respectively. The separation factor (R$_L$) value for Ag$_2$O@TNT is 0.67 and for Ag$_2$O@TNF is 0.65, which confirms the of favorability adsorption. Thermodynamic assessments show that both adsorbents undergo favorable, spontaneous, and endothermic adsorption processes, offering an efficient mechanism for I$^-$ ion extraction from aqueous solutions. A comparative assessment revealed that titanate nanotubes outperform titanate nanofibers in terms of I$^-$ ion adsorption capacity and efficiency.

✉ A. H. Hassani
    ahhassani@srbiau.ac.ir

1   Department of Environmental Science, Graduate School
    of the Natural Science and Environment, Science
    and Research Branch, Islamic Azad University, Tehran, Iran

2   Department of Environmental Engineering, Faculty
    of Natural Resources and Environment, Science and Research
    Branch, Islamic Azad University, Tehran, Iran

3   Nuclear Fuel Research School, Nuclear Science
    and Technology Research Institute, Tehran, PO
    Box 11365-8486, Iran

Graphic abstract

Adsorption of Radioactive Iodine from Wastewater by Using Ag$_2$O Titanate Nanotubes and Nanofibers
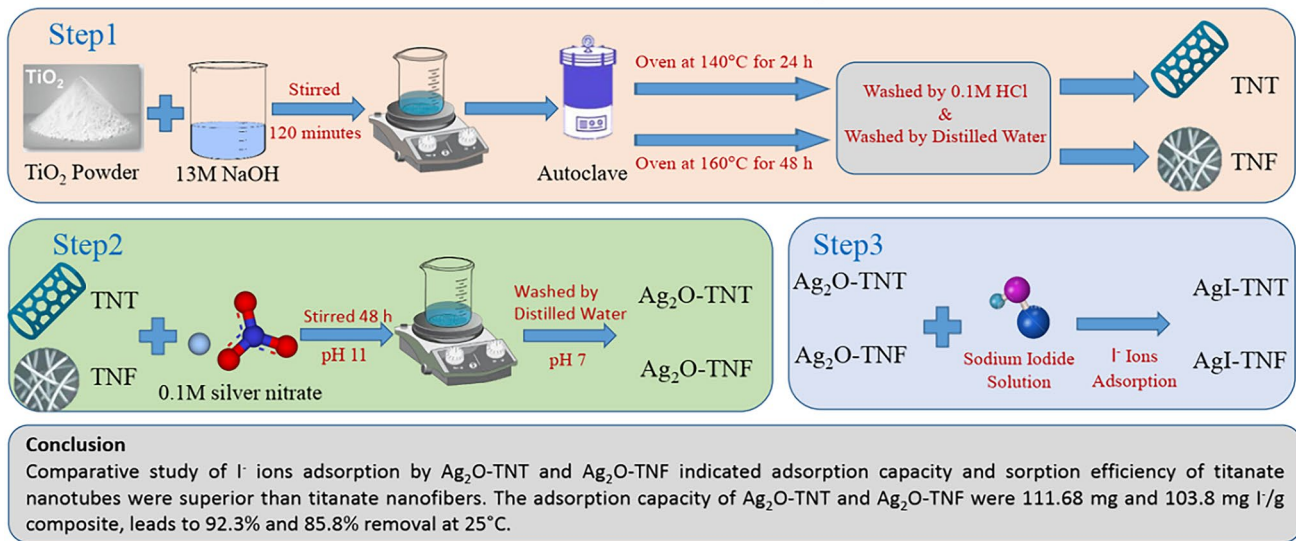
Introduction

Nuclear industries such as nuclear reactors and nuclear medical centers can release hazardous radioactive materials to the environment during normal or accident condition. Radioactive materials have the ability to damage human health due to emitting ionizing radiations, even in very low concentrations. One of the most dangerous radioactive materials is iodine, which can be released into the environment during nuclear accidents (Zhang et al. 2017). Radioactive iodine is one of the uranium fission products, which has the ability to dissolve in water and easily enter to the environment through nuclear waste leakage and an accident at a nuclear reactor (Yang et al. 2013a) such as Chernobyl, in 1986 and Fukushima, Japan in 2011. Radioactive iodine isotopes have different half-lives rang, from about 8.4 days (for ^{131}I) to 1.57×10^7 years (for ^{129}I) (Zhang et al. 2017). Not only is ^{129}I known as a deleterious long half-life time radioactive iodine isotope devastating environment owing to its high mobility and penetrating the food chain, but the short half-life radioactive iodine isotopes also cause serious devastation influence on the to the human body (Yang et al. 2013b; Yang et al. 2013a). Radioactive iodine can accumulate in the human body and lead to thyroid cancer, leukemia and metabolic disorders (Lefevre et al. 1999; Zhang et al. 2017). Therefore, considering their pernicious effects on human and environment, removal of radioactive iodine ions from the wastewater must seriously be taken into account.

Various methods have been employed for iodine removal from wastewater, including ion exchange (Decamp and Happel 2013), chemical precipitation (Mao et al. 2017), adsorption (Ikari et al. 2015) and membrane separation (Yang et al. 2016). Also, various compounds such as copper, Cu$_2$o/Cu, activated carbon and zeolite by above methods have been focused on the radioactive iodine remove (Lefevre et al. 1999; Lefèvre et al. 2000, 2003; Nguyen et al. 2012; Yuan et al. 2016; Zhang et al. 2017). In some researches, mineral materials and organic–inorganic composite adsorbents, such as Ca(ALG)$_2$–Cu$_2$O, Ca(ALG)$_2$–AgCl, Ca(ALG)$_2$–Ag, have been used to remove iodine (Zhang et al. 2012; Ikeda et al. 1994; Chmielewská-Horváthová and Lesnỳ 1995). The most common of these methods of removing iodine from aqueous solutions is adoption, due to its features such as high efficiency, low cost and easy reduction.

Previous studies have shown that I$^-$ anions easily react with silver oxide (Ag$_2$O) particles and become insoluble silver iodide (Mostata et al. 2015; Mu et al. 2017; Korobeinyk et al. 2018; Zia et al. 2021; Wang et al. 2022). However, using Ag$_2$O without applying any support can bring some disadvantages for I$^-$ adsorption procedure. The Ag$_2$O nanoparticles, due to their small size, may aggregate and form aggregated particles, which reduces the absorption of iodine. This problem could be addressed by dispersing the Ag$_2$O nanoparticles on the surface of a support material. Additionally, the separation of nanoscale adsorbents from the solution is facilitated if the sorbent molecules are fixed on the

surface of a suitable support (Yang et al. 2013a). Among the variety of support materials tested as a support of Ag$_2$O nanoparticles, TiO$_2$ exhibits good practical function. The Ag$_2$O nanocrystals have similar surfaces with the surface of the titanate nanostructures in crystallography, which means that the oxygen arrangement of Ag$_2$O is similar with the oxygen arrangement of titanate surface. Therefore, oxygen atoms are shared and bonded at the interface between the two phases, resulting in Ag$_2$O nanoparticles firmly adhering to the surface of titanate nanostructures (Bo et al. 2013). In addition, the titanate substrate has good thermal, chemical and radiochemical. TiO$_2$ nanostructures have variety of morphology such as 0D (quantum dots), 1D (nanowire, nanotubes, etc.), 2D (nanosheets, nanoflakes, etc.), and 3D (nanoparticles, nanoflowers, etc.). 1D of titanate nanostructures usually synthesized via hydrothermal method which have high specific surface area with oxygen atoms at their surfaces (Reghunath et al. 2021). The Ag$_2$O nanocrystals have similar surfaces with the surface of the titanate nanostructures in crystallography, which means that the oxygen arrangement of Ag$_2$O is similar with the oxygen arrangement of titanate surface. Therefore, oxygen atoms are shared and bonded at the interface between the two phases, resulting in Ag$_2$O nanoparticles firmly adhering to the surface of titanate nanostructures (Bo et al. 2013). In addition, the titanate substrate has good thermal, chemical and radiochemical.

Titanium dioxide (TiO$_2$) is a very versatile material that can be used to synthesize various forms of adsorbents with high specific surface such as nanowires, nanofibers, nanotubes, nanosheets, nanorods, and nanobelts (Tri Yunarti et al. 2021). The advantages of TiO$_2$ are good thermal and chemical stability, low toxicity for the environment and humans, and low cos (Almarbd and Abbass 2022). TiO$_2$ nanostructures are effective sorbents for radionuclides due to their radiochemical stability and low solubility in both acidic and alkaline solutions (Tatarchuk et al. 2019). Previous studies have shown that the addition of Ag$_2$O to synthesized TiO$_2$ nanoabsorbents is feasible, as it does not affect their crystal structure or morphology (Tri Yunarti et al. 2021).

There are a number of research conducted on adsorption of iodine ions by attaching Ag$_2$O particles on the large surface area adsorbents so that, the attached Ag$_2$O centers absorb I$^-$ ions from wastewater. The adsorption of iodine ions by grafted titanate nano-lamina and layered sodium vanadate-based sorbents are previously reported (Bo et al. 2013; Sarina et al. 2014). In similar studies, the adsorption of iodine ions using silver oxide titanat nanotube and silver oxide titanat nanofiber which were synthesized by hydrothermal method have also been reported, (Yang et al. 2008; Yang et al. 2011; Yang et al. 2013a; Yang et al. 2013b). Previous studies in BET analysis of TiO$_2$ nanoparticles shows, its specific surface area is 50 m^2.g^{-1}. But after hydrothermal treatment and morphology change and the formation of

titanate nanotubes and nanofibers, the specific surface area becomes larger (Davit et al. 2004; Reghunath et al. 2021). Therefore, the advantage of nanotubes and nanofibers morphology compared to TiO$_2$ nanocrystals is to increase the specific surface area. The increase in the specific surface area provides the conditions for more binding of the Ag$_2$O nanocrystals on their surface and ultimately leads to more iodine absorption.

In this study, it has been tried to synthesize Ag$_2$O@TNT and Ag$_2$O@TNF with efficient absorption by changing the synthesis method of previous studies. The applied changes include increasing the concentration of NaOH from 10 to 15 M (increasing alkalinity) and increasing the hydrothermal temperature in two stages. Also, Characterization of synthesized Ag$_2$O@TNT and Ag$_2$O@TNF adsorbents and the effect of various adsorption parameters such as contact time, adsorbent concentration, temperature, pH and iodine ion concentration of aqueous solutions, furthermore, were investigated. The equilibrium results correlated with diverse isotherm models (Langmuir, Freundlich and Temkin), kinetic and thermodynamic parameters have been studied in detail. In addition, a feasibility study on the real waste of a radiopharmaceutical production center was performed and the results indicated that ^{131}I has been absorbed by Ag$_2$O@TNT and Ag$_2$O@TNF and the activity of the ^{131}I has decreased after equilibrium.

Materials and methods

All the chosen reagents were of analytical grade and purchased from Merck Company. The solutions were prepared with deionized water (DW). The iodine solution stock was prepared by dissolving NaIO$_3$ in DW. The Ag$_2$O particle was prepared by dissolving AgNO$_3$ in DW. TiO$_2$ powder and NaOH were used for TNT and TNF nanostructure synthesis. The initial pH of solutions was regulated by nitric acid (HNO$_3$; 99.9%) or sodium hydroxide (NaOH; 99.9%) solutions and Metrohm pH meter model 744. Sartorius Electrical Balance model ED224S, Laboren Oven, Centrifuge model Rotina 380, Heater & stirrer IKA RCT basic, and thermometer model Testo 106 were used for conducting the experiments. Synthesis of adsorbent was done by using hydrothermal reactor, which was designed and made of stainless steel 316 L as well as conventional autoclaves with Teflon liner by volume of 200 ml. Characterizations of the synthesized adsorbents were determined by XRD model STADI MP-STOE Company (Germany), FT-IR model Vector22 Brucker Company (USA), SEM model Zeiss EVO18 (Germany), TEM model PHILIPS-EM 208 (Netherland) and BET model Quantachrome NOVA 2.2 system (USA). Titration Set model Metrohm titron plus 848 was used for I-ion concentration analysis (Swiss).

Synthesis of Ag$_2$O@TNT and Ag$_2$O@TNF

Ag$_2$O@TNT and Ag$_2$O@TNF were synthesis by the high alkalinity hydrothermal method. At the first step, 5 g of TiO$_2$ powder was mixed with 150 ml of 15 M NaOH solution and stirred at room temperature by a magnetic stirrer for 120 min, then transferred to an ultrasonic bath for 30 min to obtain a homogeneous solution. In the second step, the mixture was poured into a 200 ml stainless steel hydrothermal reactor with a PTEE container inside. The hydrothermal reactor was heated in an oven first at 100 °C for 12 h, then the temperature was increased to 130 °C for 12 h for titanates nanotube. For titanates nanofibers synthesis, the hydrothermal reactor was heated in an oven first at 120 °C for 12 h, then the temperature was increased to 150 °C for 12 h. After the heating process, the hydrothermal reactor was left in the oven for a further 24 h, and the temperature gradually decreased. Then, the TNT or TNF precipitate was washed once with 0.1 M HCl solution and several times with distilled water until the pH of the solution remaining from washing step reach to about 7. The TNT and TNF precipitate were collected by centrifuging and then dried in oven at 50 °C for 24 h.

In the third step, in order to synthesize Ag$_2$O@TNT and Ag$_2$O@TNF, the Ag$_2$O particles were deposited on TNT and TNF as follows: 5 g of TNT or TNF was added in 450 ml of 0.1 M silver nitrate (AgNO$_3$) solution, and a 0.1 M NaOH solution was added dropwise to the reaction container in order to adjust the pH value to 12. Then, the mixture was stirred for 60 h at room temperature to complete the reaction and firmly bind Ag$_2$O particles on the TNT and TNF surface. Then, the precipitates were collected and washed with distilled water until the pH value fixed to about 7. Finally, Ag$_2$O@TNT and Ag$_2$O@TNF precipitate were dried in an oven at 50 °C for 24 h. Summarized steps of the synthesis Ag$_2$O@TNT and Ag$_2$O@TNF as follows:

Adsorption experiments

The adsorption experiments of this research were implemented on batch technique with nonradioactive I$^-$ ions in aqueous solution in a flask. The solution containing of I$^-$ ion (50–350 ppm) was mixed with the 0.05 g of adsorbent at contact time (2–120 min) and pH values (3–10). The flask was placed in a heater stirred at 150 rpm. The initial pH of I$^-$ solutions was adjusted by adding 0.01 M HNO$_3$ or NaOH solutions. Following the adsorption experiments and after equilibrium, the samples were centrifuged at 4000 rpm for 20 min to separate the solid and liquid phases. Then, the residual concentration of the iodine ions was determined by using the potentiometric titration method with a silver electrode and a silver nitrate solution by Metrohm Auto-Titration Set. The equilibrium uptake (q$_e$ mg.g^{-1}) and removal efficiency or uptake (%R) of the iodine ions were calculated according to the Eqs. (1) and (2), respectively:
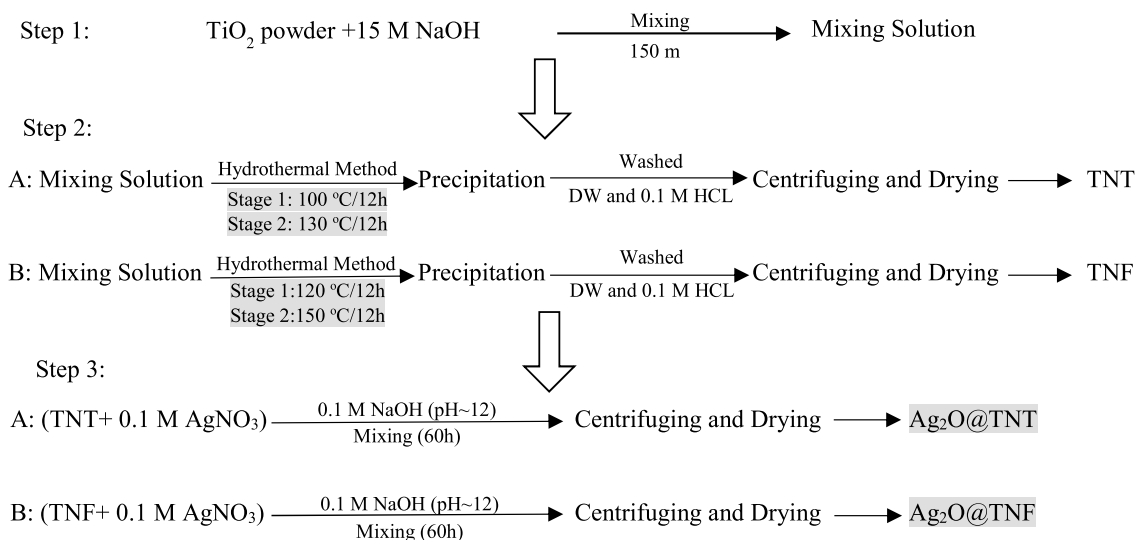
$$q_e = \frac{C_0 - C_e}{m} \times V \tag{1}$$

$$R\% = \frac{C_0 - C_e}{C_0} \times 100 \tag{2}$$

where C_0 and C_e (mg/L) are the initial and equilibrium metal ion concentrations, respectively, V and m are the liquid volume (L) and the weight of dried used adsorbent (g).

Desorption experiments

Desorption experiments were investigated in batch system using pure water and 0.1 M aqueous solutions of NaCl and

Step 1:   TiO$_2$ powder +15 M NaOH —— Mixing / 150 m ——▶ Mixing Solution

Step 2:

A: Mixing Solution —— Hydrothermal Method / Stage 1: 100 °C/12h / Stage 2: 130 °C/12h ——▶ Precipitation —— Washed / DW and 0.1 M HCL ——▶ Centrifuging and Drying ——▶ TNT

B: Mixing Solution —— Hydrothermal Method / Stage 1:120 °C/12h / Stage 2:150 °C/12h ——▶ Precipitation —— Washed / DW and 0.1 M HCL ——▶ Centrifuging and Drying ——▶ TNF

Step 3:

A: (TNT+ 0.1 M AgNO$_3$) —— 0.1 M NaOH (pH~12) / Mixing (60h) ——▶ Centrifuging and Drying ——▶ Ag$_2$O@TNT

B: (TNF+ 0.1 M AgNO$_3$) —— 0.1 M NaOH (pH~12) / Mixing (60h) ——▶ Centrifuging and Drying ——▶ Ag$_2$O@TNF

HNO$_3$. The AgI@TNT and AgI@TNF adsorbents saturated with I$^-$ ions were placed in contact with the desorption solution for 12 h and 24 h at room temperature. Then Auto-Titration Set measured the concentrations of I$^-$ ions released into the solution.

Results and discussion

Characterization of adsorbents

XRD analysis

Characterization of the crystalline phase of the synthesized TNT, Ag$_2$O@TNT, AgI@TNT (a) and TNF, Ag$_2$O@TNF, AgI@TNF (b) were determined by X-ray powder diffract meter (STV_MP STOE Company, Germany) and their patterns are shown in Fig. 1a and b. In this study, Cu Kα radiation (λ = 1.5405 Å) was used, and the samples were scanned in a 2θ range angles from 5 to 99° at a scanning rate of 0.015°/S. The XRD analyses of both TNT and TNF show the peak are included anatase (A) and rutile (R) structure (Liu et al. 2013a, b, c; ElShorafa et al. 2023). The peaks at 2θ ≈ 25.3°, 38.4°, 48.35°, and 52.39°, which correspond to the planes (101), (004), (200), and (105), identified the anatase structure, according to JCPDS file No. 021-1272 (Emran and Alsahli 2021; Sun et al. 2015). The peaks at 2θ ≈ 29° and 35°, which correspond to planes (101), (110), determined the Rutile structure (ElShorafa et al. 2023). The diffraction peaks attributed to anatase and rutile of TNT and TNF are according to JCPDS file No. 75-1537 (Morad et al. 2020). The XRD analyses of both TNT and TNF show a distinct peak at 2θ° ≈ 10 which correspond to the plane (100), can be attributed to interlayer space of TNT and TNF (Liu et al. 2013a, b, c). In addition,

this plane confirms that titanate materials are formed by the octahedron slab unit (Bo et al. 2013). Moreover, peaks at 2θ ≈ 32° and 38° which correspond to the planes (111), (200), were assigned to Ag$_2$O indexed according to JCPDS file No. 76-1393 (Gao et al. 2017; Villavicencio et al. 2020). The diffraction peaks situated at 2θ ≈ 22.40°, 23.70°, 25.31°, 39.25° and 46.35°, are corresponding to the planes (100), (002), (101), (110), (112) were assigned to AgI indexed according to JCPDS file No. 09-0374 (Cheng et al. 2013; Khan et al. 2019; Chao et al. 2020).

When Ag$^+$ ions are spread onto the TNT and TNF titanate surface in a neutral condition, silver hydrate intermediates, Ag(OH)n(H$_2$O)m, are formed. The silver hydrate intermediates, dehydrate by sharing surface oxygen atoms of the TiO$_6$ octahedron slabs plane (100) bond on the TiO$_6$ octahedra. Due to the sharing of surface oxygen atoms, a serious deformation of the surface plane (100) occurs, and as a result, the diffraction intensity of this plane decreases. On the other hand, the exchange of Ag$^+$ ions with Na$^+$ ions in the interlayer space, causes the deterioration of crystallinity and the reduction of diffraction intensity. When the iodine ions diffuse onto the Ag$_2$O nanocrystals, I$^-$ ions capture by Ag$_2$O and convert to AgI nanocrystals on the titanate surface of TNT and TNF absorbents. When iodine ions spread on Ag$_2$O nanocrystals placed on the surface of TNT and TNF, I$^-$ ions are absorbed by Ag$_2$O and become AgI nanocrystals. AgI nanocrystals are attached firmly to the surface of TNT and TNF through binding of silver atoms to oxygen atoms of Ti–O frameworks (Yang et al. 2011).

According to Fig. 1, the diffraction peaks of TNT and TNF remain after adding Ag$_2$O, but their intensity has decreased due to the exchange of Na$^+$ ions with Ag + ions (Li et al. 2012; Xu et al. 2012). Furthermore, comparison of XRD patterns indicates that Ag$_2$O has been attached on TNT and TNF and I$^-$ ions are attached to silver.
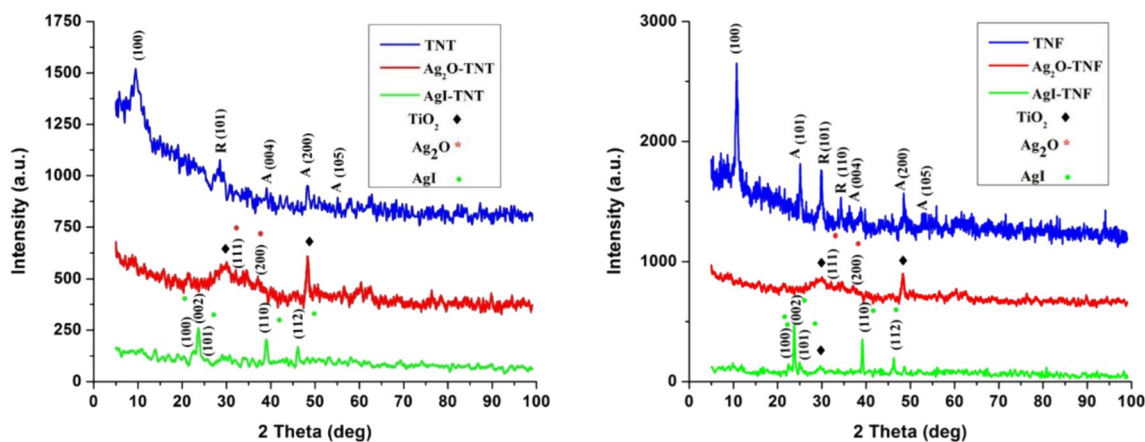

Fig. 1 XRD graphs of (**a**) for TNT, Ag$_2$O@TNT, and AgI@TNT, as well as (**b**) for TNF, Ag$_2$O@TNF and AgI@TNF

FT-IR analysis

The structure of Ag$_2$O@TNT and Ag$_2$O@TNF adsorbents was confirmed by FT-IR analysis. The FT-IR spectra are in the range between 400 and 4000 cm^{-1}, and the results have been illustrated in Fig. 2a and b, respectively. The absorption peak at 400–800 cm^{-1} corresponded to the stretching vibration of Ti–O or Ti–O–Ti (Rodrigues et al. 2010; Sheng et al. 2012; Abbasizadeh et al. 2013). The peak obtained in the region of 3200–3550 cm^{-1} corresponded to the stretching vibration of hydroxyl groups (O–H), which show the presence of water on the surface and interlayer space. The peak of 1600–1650 cm^{-1} also confirmed the presence of water, which is related to the H–O–H bending vibrations of water molecules (Emadzadeh et al. 2015; GallardoáAmores et al.

1994; Peng et al. 1995). The strongest peak in the range of 513–550 cm^{-1} can correspond to the stretching vibration of the Ag–O group (Yong et al. 2013).

SEM and TEM analysis

The morphology of Ag$_2$O@TNT and Ag$_2$O@TNF was characterized by SEM and TEM. Figure 3a and b shows high-resolution SEM images of Ag$_2$O@TNT and Ag$_2$O@TNF for surface analysis details. These details include particle distribution, morphology, surface structure and particle size of the adsorbents. The SEM image confirmed that more Ag$_2$O@TNT and Ag$_2$O@TNF nanostructures were synthesized in the form of two-dimensional tube and fiber species. The SEM images indicate that the diameter Ag$_2$O@

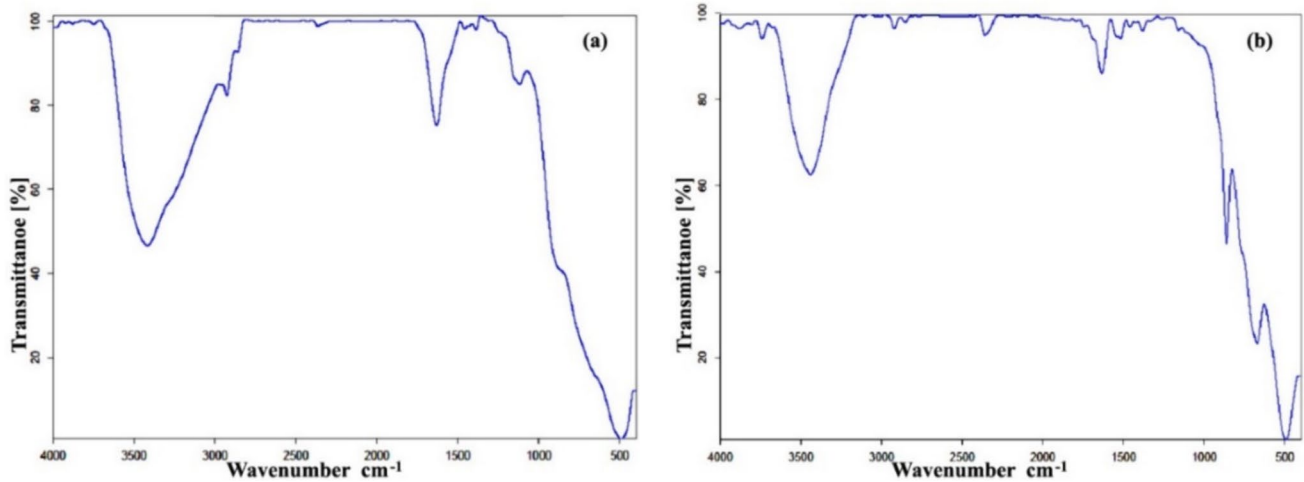**Fig. 2** FT-IR graphs of (**a**) Ag$_2$O@TNT and (**b**) Ag$_2$O@TNF
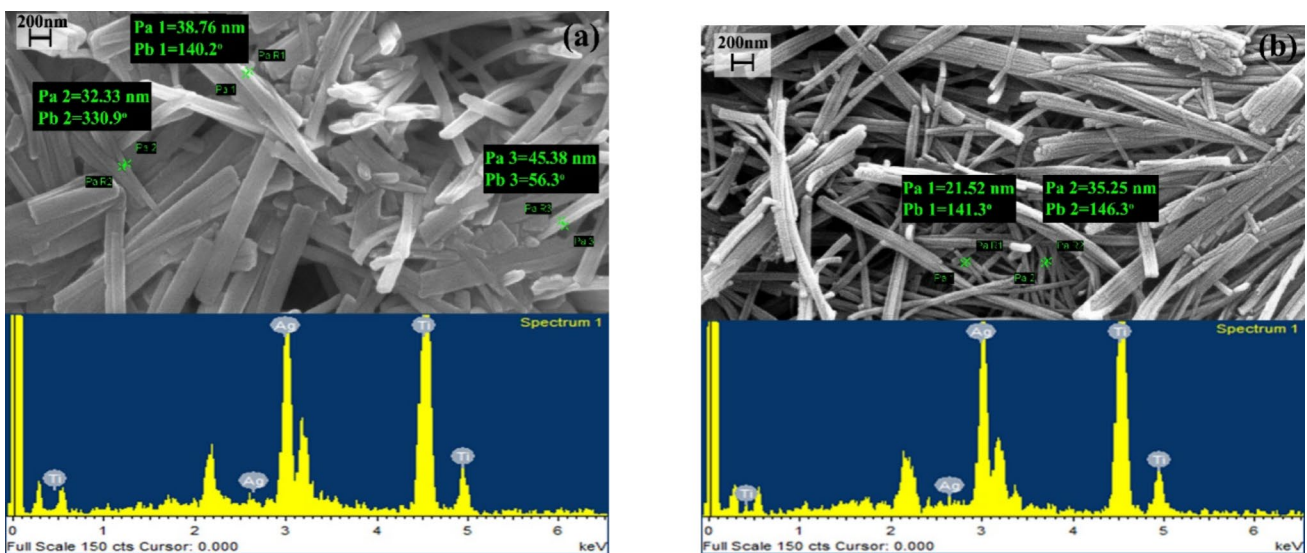
Fig. 3 SEM images of (**a**) Ag$_2$O@TNT and (**b**) Ag$_2$O@TNF

TNT and Ag$_2$O@TNF are interlaced each other and length of Ag$_2$O@TNT distribution within 32–45 nm, 45–170 nm and for Ag$_2$O@TNF 21–35 nm and 51–185 nm (Zima et al. 2012; Zhang et al. 2015; Xu et al. 2012; Okada et al. 2015; Filipowicz et al. 2014).

TEM images of Ag$_2$O@TNT, Ag$_2$O@TNF is shown in Fig. 4a and b. TEM images illustrating the Ag$_2$O nanocrystals distributed on the external surface of the titanate nanotubes and nanofibers. Also, the TEM images indicated that AgI crystals are attached to the titanate nanotubes and nanofibers (Yang et al. 2011; Yang et al. 2013b; Okada et al. 2015; Filipowicz et al. 2014; Liu et al. 2013a, b, c).

BET analysis

Surface areas and pore volumes analysis The specific surface area of Ag$_2$O@TNT and Ag$_2$O@TNF sorbents were determined by the Brunauer–Emmett–Teller (BET) through nitrogen adsorption isotherms. Moreover, the average pore size distribution of Ag$_2$O@TNT and Ag$_2$O@TNF was characterized by Barrett–Joyner–Halenda (BJH) method. The specific surface area and pore size distribution of the samples are presented in Table 1. The comparison BET surface area and the I$^-$ removal capacity of Ag$_2$O@TNT and Ag$_2$O@TNF and other Ag$_2$O-based adsorbents are presented in Table 4.

One of the advantages of the TNT and TNF compared to spherical TiO$_2$ morphology is the increase in specific surface area. The BET analysis of TiO$_2$ nanoparticles shows, its specific surface area is 50 m^2.g^{-1}. The BET analysis of synthesized Ag$_2$O@TNT and Ag$_2$O@TNF adsorbents for this work show the specific surface area of them are about 105.4 and 80.5 m^2.g^{-1}. Therefore, the advantage of nanotubes and nanofibers morphology compared to TiO$_2$ nanocrystals is to increase the specific surface area. The increase in the specific surface area provides the conditions for more binding of the Ag$_2$O nanocrystals on their surface which can ultimately lead to more I$^-$ absorption.

Table 1 Specific surface area and pore size distribution of Ag$_2$O@TNT and Ag$_2$O@TNF

Nanostructure	Specific surface area (m^2.g^{-1})	Pore size (nm)
Ag$_2$O@TNT	105.4	3.078
Ag$_2$O@TNF	80.5	3.078

Zeta-potential analysis

In order to study the zeta-potential, the synthesized Ag$_2$O@TNT and Ag$_2$O@TNF nanoadsorbents were dispersed in double distilled water. The stability of nanoparticles depends upon the electrical potential and the surface charge. The surface potential of charge particle increases with increase in zeta potential. The zeta potential of synthesized Ag$_2$O@TNT and Ag$_2$O@TNF nanoadsorbents are − 12.5 mV and − 23.3 mV respectively, as shown in the Fig. 5a and b.

Adsorption properties of Ag$_2$O@TNF and Ag$_2$O@TNT

Effect of pH

The pH value is one of the important parameters in changing the adsorption of ions on adsorbents. The effect of pH on the adsorption of I$^-$ on Ag$_2$O@TNT and Ag$_2$O@TNF was investigated in the pH range of 3–10, at 25 °C, 0.05 g adsorbents, 100 mgL^{-1} initial I$^-$ ions concentration and contact time of 30 min. The 0.1 M HNO$_3$ and 0.1 M NaOH solution have been used to change and adjust the pH value. In each test, after 30 min, the precipitate was collected by centrifuging for about 20 min, and the concentration of I$^-$ ions after equilibrium sorption was determined by potentiometric titration method with silver electrode and silver nitrate solution.

As shown in Fig. 6a, the ability of I$^-$ anion absorption by Ag$_2$O@TNT and Ag$_2$O@TNF decreases in acidic media, especially at pH ≤ 3, due to the change in the structure of
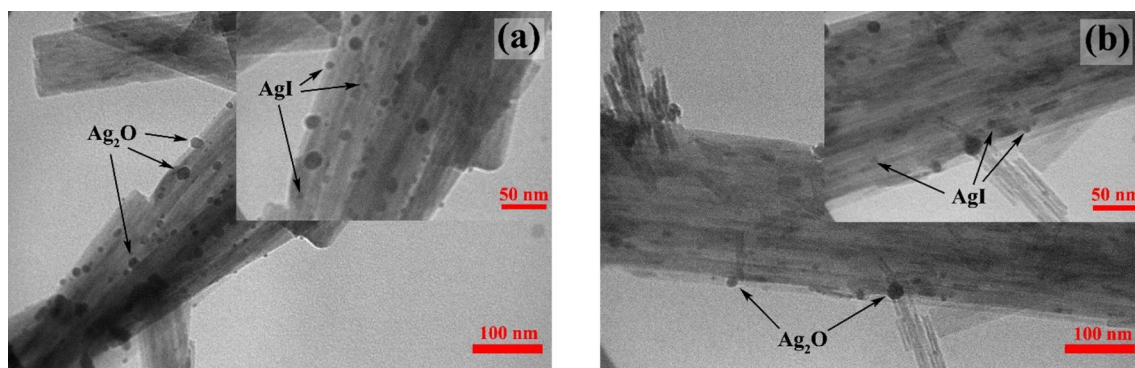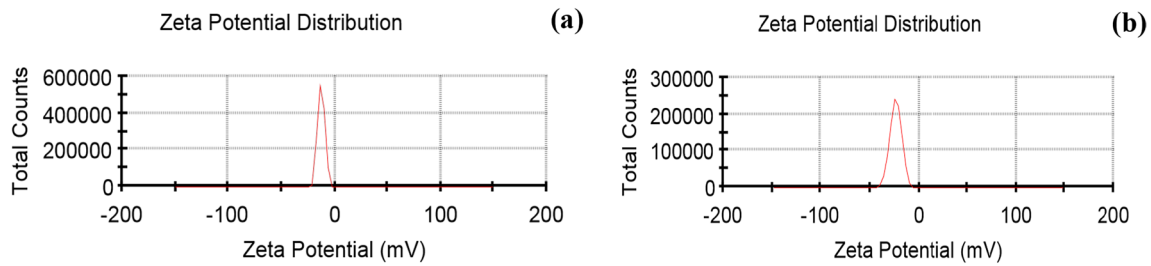

Fig. 4 TEM images of (**a**) Ag$_2$O@TNT and (**b**) Ag$_2$O@TNF

Fig. 5 Zeta potential of synthesized Ag$_2$O@TNT (**a**) and Ag$_2$O@TNF (**b**) nanoadsorbents
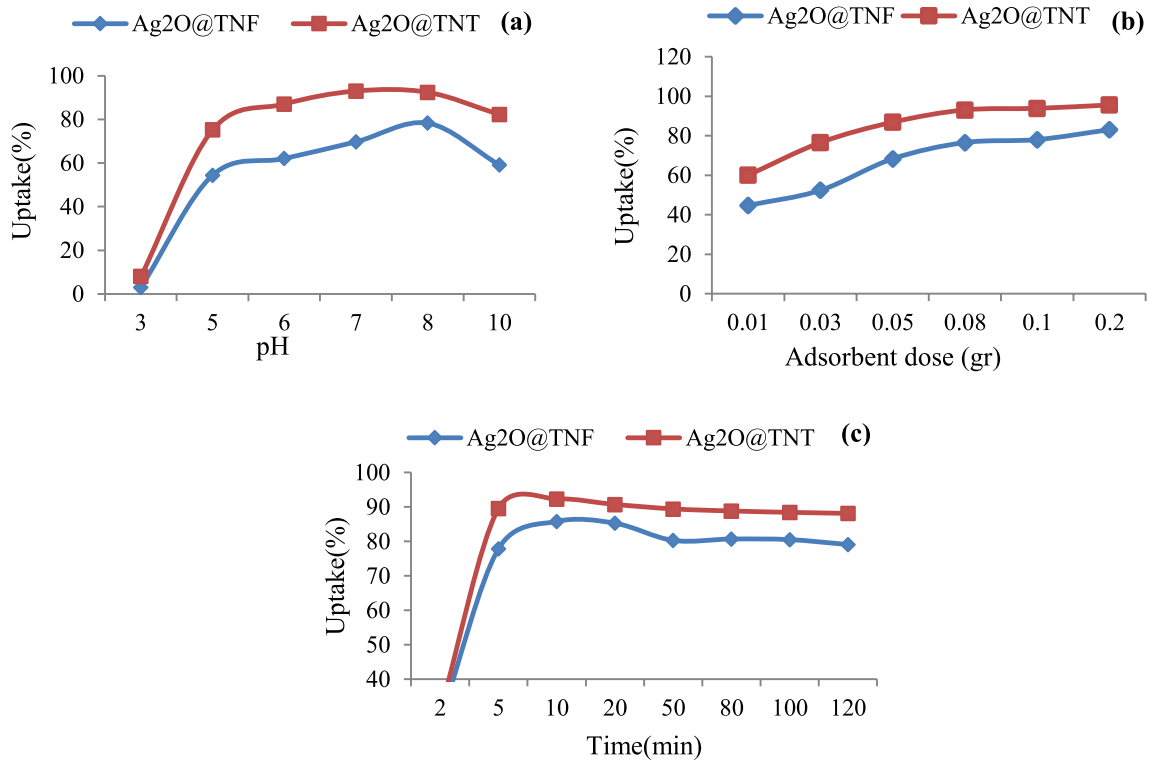

Fig. 6 Optimization of adsorption parameters: pH (**a**), adsorbent dosage (**b**) and time (**c**)

these nanoparticles. This phenomenon has been reported in previous literatures (Mu et al. 2016). In addition, under basic condition (pH > 9), the uptake ability of the Ag$_2$O nanoparticles decreased again because of hydroxide ion competition.

The pH changes, have a very important effect on the synthesis process of TNT and TNF, alkaline pH causes TiO$_2$ bonds to break, and acidic pH during acid washing causes rolling and formation of nanotubes or nanofibers. When strong NaOH combines with TiO$_2$, some of the Ti–O–Ti bonds are broken and an intermediate compound containing Ti–O–Na and Ti–OH is formed. Then this intermediate compound forms a layered structure whose main units are TiO$_6$-octahedra. TiO$_6$ octagons, by sharing common edges with other octagons, form thin zigzag layers with

Na$^+$ and OH$^−$ between them. Washing with acid causes Na$^+$ in between the layers to be replaced by H$^+$, which process changes the surface charge of the layers and separates the titanate layers from each other and rolls and transforms the layers into titanate nanotubes and titanate nanofibers (Tsai and Teng 2006; Nhat and Hsunling 2015; Hsin-Hung and Shang-Lien 2007).

Effect of adsorbent dosage

Adsorbent dose is one of the basic parameters in adsorption processes. The effect of adsorbent dose on absorption rate was tested and investigated by using different amounts of synthesized Ag$_2$O@TNT and Ag$_2$O@TNF (0.01, 0.03, 0.05,

0.1 and 0.2 g) at 25 °C, 0.05 g adsorbents, 100 mgL^{-1} initial I$^-$ ions concentration and contact time of 30 min as shown in the Fig. 6b. The optimal dose of adsorbent was obtained after using 0.05 g of adsorbent. As the figure illustrates, the ability to remove I$^-$ ions by Ag$_2$O@TNT and Ag$_2$O@TNF increases with increasing adsorbent dosage due to the increased availability of active sorption positions.

Effect of contact time and kinetic modeling

Contact time plays an important role in the investigate adsorption kinetics. The adsorption kinetics of I$^-$ ions on Ag$_2$O@TNT and Ag$_2$O@TNF were studied as a function of contact time varying from 2 to 120 min. For this experiment, 0.01 g of Ag$_2$O@TNT or Ag$_2$O@TNF adsorbents were added to 20 ml of NaI solution with an initial I$^-$ ion concentration of 100 mg/L in a flask at a temperature of 25 °C and pH 7.

Figure 6c, illustrates the results of these experiments, at the beginning of contact with the adsorbent, the rate of absorption of I$^-$ ions are fast because of more available active reactants (Ag$_2$O), but after about 10 min, the rate of absorption decreases due to active gradual occupancy of the sites until it reaches equilibrium, this occurred after about 30 min. At equilibrium, the uptake percentage of I$^-$ ions by Ag$_2$O@TNT was 93.2%, and by Ag$_2$O@TNF was 72.5%.

Kinetic models describe the mechanism of the adsorption process. In this work, the experimental data were used to interpret the kinetic data, applying two pseudo-first and second-order kinetic models as Eqs. (3) and (4), respectively (Ho and McKay 1998, 1999):

$$q_t = q_e - q_e \exp(-k_1 t) \tag{3}$$

$$\frac{t}{q_t} = \frac{1}{k_2 q_e^2} + \frac{t}{q_e} \tag{4}$$

where q_t and q_e (mg. g^{-1}) are the I$^-$ uptakes at time t (min) and at equilibrium, respectively, and k_1 (min^{-1}) and k_2 (g. mg^{-1} min^{-1}) are the corresponding rate constants.

The kinetic results show that the adsorption of I$^-$ ions on Ag$_2$O@TNF and Ag$_2$O@TNT are fast and the adsorption rate can be fitted with a pseudo-second-order kinetic model with high correlation coefficients ($R^2 = 0.9991$ for Ag$_2$O@TNT) and ($R^2 = 0.9983$ for Ag$_2$O@TNF). The values of q_e, k_1, k_2, and correlation coefficient (R^2) of both Ag$_2$O nano-titanate are presented in Table 2, which were calculated using the slope and intercept of the lines in Fig. 7a and b. The findings show that the absorption kinetics corresponds to a pseudo-second-order model and shows that the R^2 value is satisfactory and linear.

Table 2 Parameters of pseudo-first and second-order models of I$^-$ ions adsorption onto Ag$_2$O@TNT and Ag$_2$O@TNF

Adsorbents	Kinetic model					
	Pseudo-first-order			Pseudo-second-order		
	q_e(mg. g^{-1})	K_1(min^{-1})	R^2	q_e(mg. g^{-1})	K_2(g. mg^{-1} min^{-1})	R^2
Ag$_2$O@TNT	10.3633	-0.05204	0.2693	8.06451	0.78859	0.9991
Ag$_2$O@TNF	14.30869	-0.05319	0.2618	6.61813	1.56378	0.9988
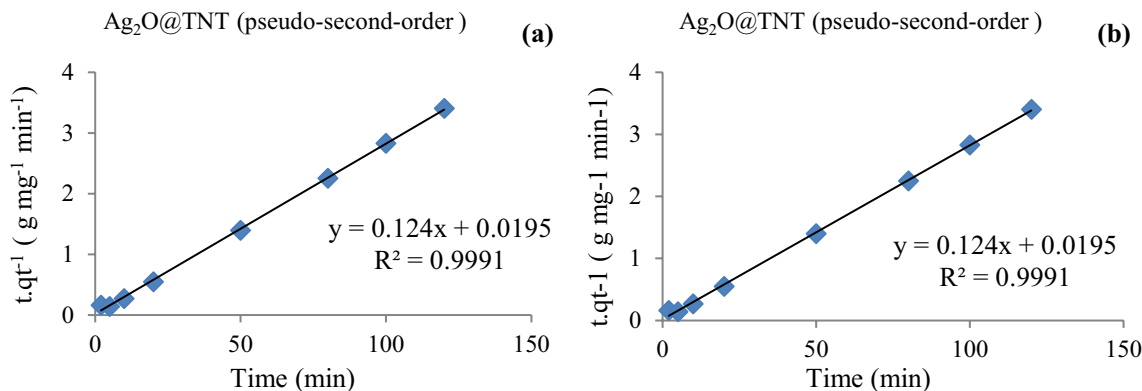
Fig. 7 Pseudo-second-order kinetics for I$^-$ ions (**a**) Ag$_2$O@TNT and (**b**) Ag$_2$O@TNF powder

Effect of initial ions concentration and adsorption isotherms

The effect of the initial ion concentration is an important parameter to check and determine the absorption capacity of the adsorbent. To study the adsorption isotherms, the initial ion concentration parameter has been used and Langmuir, Freundlich and Temkin isotherm models have been utilized to determine the adsorption isotherm of I^- ions in $Ag_2O@$ TNT and $Ag_2O@$TNF. For this purpose, 20 ml of NaI solution with different initial I^- ions concentrations ranging from 100 to 350 mg L^{-1} were prepared. Then 0.05 g of $Ag_2O@$TNT or $Ag_2O@$TNF adsorbents were added in a flask at 25 °C temperature, contact time 30 min, and the optimized pH values 7.

Figure 8 shows that the adsorption capacity of $Ag_2O@$TNT and $Ag_2O@$TNF decreases after the concentration of 100 mg L^{-1} of I^- ions, due to the occupation of the adsorption sites by I^- ions. Therefore, 100 mg L^{-1} of I^- ions concentration was selected as an optimum concentration.

Langmuir adsorption isotherm model

The Langmuir adsorption isotherm theory describes the process by which the amount of a layer of an adsorbent that forms on the outer surface of the adsorbent. After the absorption layer is formed on the absorbent surface, no further absorption occurs and the absorption capacity of the absorbent is completed (Dada et al. 2012). Equation (5) provides the linear expression of the Langmuir isotherm model (Kowanga et al. 2016):

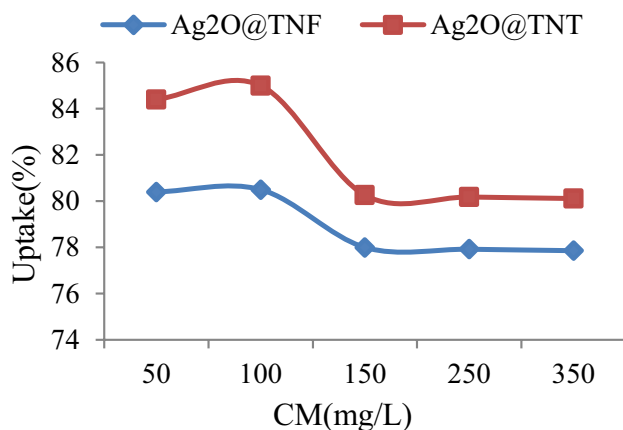$$\frac{C_e}{q_e} = \frac{1}{K_L q_e} + \frac{1}{q_{max}} C_e \tag{5}$$

Fig. 8 Effect of initial concentration on the absorption of I^- ions by $Ag_2O@$TNT and $Ag_2O@$TNF powder

In this context: C_e it shows the equilibrium concentration of the adsorbate (mg L^{-1}); q_e signifies the amount of ion adsorbed for each gram of adsorbent at equilibrium (mg g^{-1}); q_{max} to express the peak monolayer coverage ability (mg g^{-1}); and K_L denotes the constant associated with the Langmuir isotherm (L mg^{-1}). The q_{max} and K_L values can be obtained from the slope and y-intercept of the Langmuir linear plot (C_e/q_e) against C_e, depicted in Fig. 9. The details of Langmuir isotherm parameters are presented in Table 3. The adsorption tendency between the adsorbed substance and the adsorbent can be predicted using the separation factor (R_L). R_L provides important information about the specificity of the absorption process. The R_L value indicates whether the type of isotherm is favorable ($0 < R_L < 1$) or not ($R_L > 1$), while an RL value of 1 indicates linear adsorption and 0 indicates irreversible adsorption. The separation factor equation is mentioned in Eq. (6) (Kowanga et al. 2016):

$$R_L = \frac{1}{1 + K_L C_0} \tag{6}$$

In this equation, K_L is the Langmuir constant, and C_o is the initial concentration of the ion.

Freundlich adsorption isotherm model

A Freundlich adsorption isotherm model is used to describe the adsorption characteristics of heterogeneous surface (Dada et al. 2012).

The linear form of the Freundlich adsorption isotherm model is presented mathematically with the Eq. (7) (Kowanga et al. 2016):

$$\log q_e = \log k_f + \frac{1}{n} \log C_e \tag{7}$$

where q_e is the amount of adsorbed ions at equilibrium (mg g^{-1}), K_f is the Freundlich constant related to sorption capacity (mg g^{-1}), 1/n is the intensity of the adsorption, and C_e is the equilibrium concentration of adsorbate (mg L^{-1}).

The linear Freundlich graph, plotting log q_e against log C_e as depicted in Fig. 9, therefore, the values of 1/n and kf can be determined from its gradient and y-intercept, respectively. Table 3 lists the Freundlich isotherm parameter details.

Temkin adsorption isotherm model

The Temkin adsorption isotherm theory states that the heat of adsorption for all molecules in the layer decreases linearly as opposed to logarithmically with the coverage (Dada et al. 2012). Equation (8) presents the linear isotherm of Temkin adsorption (Dada et al. 2012):
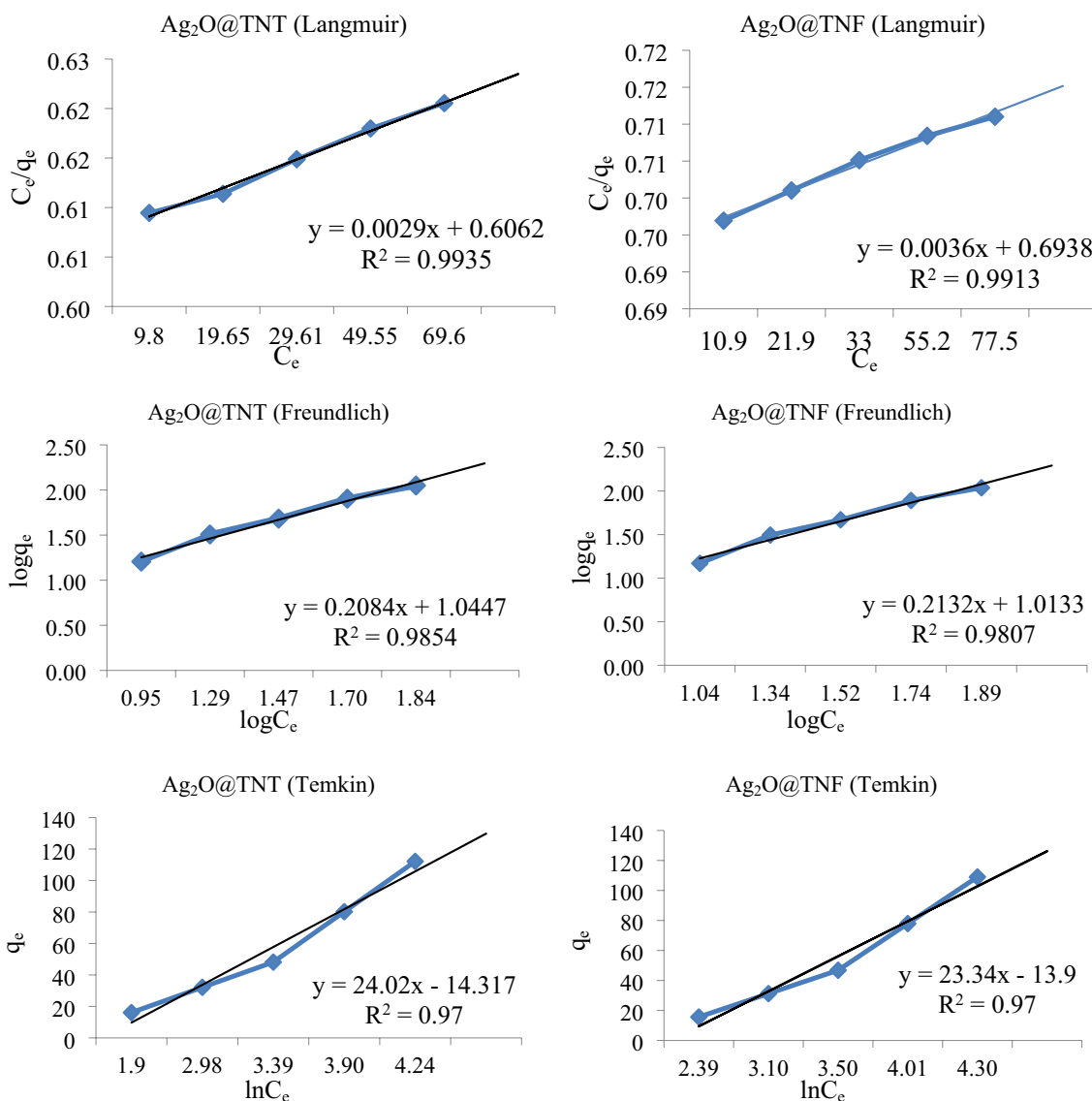
Fig. 9 Langmuir, Freundlich and Temkin adsorption isotherm plots for the sorption I⁻ ions on the Ag₂O@TNT and Ag₂O@TNF

Table 3 Parameters of Langmuir, Freundlich and Temkin adsorption isotherm models of I⁻ ions adsorption onto Ag₂O@TNT and Ag₂O@TNF

Adsorbents	Isotherm models									
	Langmuir parameters				Freundlich			Temkin		
	q_{max} (mg. g^{-1})	K_L (L.mg^{-1})	R_L	R^2	K_f (mg.g^{-1})	n	R^2	A_T (L.g^{-1})	b_T (kJ.mol^{-1})	R^2
Ag₂O@TNT	344.83	0.0048	0.67	0.9935	11.084	4.898	0.9854	1.8148	103.147	0.97
Ag₂O@TNF	277.77	0.0052	0.65	0.9913	10.310	4.690	0.9807	1.8139	106.151	0.97

$$q_e = \frac{RT}{b_T} \ln A_T + \frac{RT}{b_T} \ln C_e \qquad (8)$$

where q_e is the amount adsorbed at equilibrium (mg g^{-1}), A_T is Temkin isotherm equilibrium binding constant (L g^{-1}), b_T is Temkin isotherm constant (kJ mol^{-1}), RT is the universal gas constant (8.314 J mol^{-1} K^{-1}), T is the temperature at 298 K, and C_e is the equilibrium concentration of adsorbate (mg L^{-1}).

The values of A_T and b_T were determined from the slope and intercept of the linear Temkin plot of q_e versus Ln C_e,

as shown in Fig. 9. The values of Temkin isotherm parameters are presented in Table 3.

Based on the correlation coefficients and experimental data of this study, the R^2 values of the Langmuir Isotherm model are 0.9935 and 0.9913 for I^- ions adsorption on $Ag_2O@TNT$ and $Ag_2O@TNF$, respectively. Therefore, the Langmuir isotherm model fits the adsorption data better than the Freundlich and Temkin models. These results indicate I^- ions adsorption on the $Ag_2O@TNT$ and $Ag_2O@TNF$ occurs with the formation of monolayer adsorption.

R_L values are in the range of 0 to 1, which shows that $Ag_2O@TNT$ and $Ag_2O@TNF$ are effective adsorbents for I^- ions and the absorption process is favorable and irreversible.

Table 4. Comparison of the maximum I^- adsorption capacities, pH and BET of $Ag_2O@TNT$ and $Ag_2O@TNF$ and other Ag_2O-based adsorbent in previous studies. The comparison of the results shows that $Ag_2O@TNT$ and $Ag_2O@TNF$ have an acceptable absorption capacity for I^- ions, therefore, these adsorbents prepared in this study have the potential to be an efficient adsorbent for the removal of I^- ions.

According to the BET results and the maximum adsorption capacity of the synthesized nanosorbents, it can be concluded that due to the greater surface area of $Ag_2O@TNT$ than $Ag_2O@TNF$, more Ag_2O nanoparticles are placed on its surface and as a result, I^- ions more were absorbed by $Ag_2O@TNT$.

Effect of temperature and thermodynamic studies

In thermodynamic studies, the effect of temperature on the adsorption of I^- ions on $Ag_2O@TNT$ and $Ag_2O@TNF$ adsorbents were investigated in the temperature range of 15, 25, 30, 40, 50 and 60 °C, while other parameters were optimal, In the conditions that other studied parameters were in optimum value mode as shown in the Fig. 10.

To investigate the absorption process, thermodynamic parameters such as enthalpy change $\Delta H°$ (kJ mol^{-1}), entropy change $\Delta S°$ (kJ mol^{-1} K^{-1}) and free energy change ($\Delta G°$) which describe the adsorption of ions on $Ag_2O@TNT$ and $Ag_2O@TNF$ are taken into account Eq. (9) (Piccin et al. 2011; Erhayem et al. 2015; Atta and Akl 2015):

$$\ln K_d = \frac{\Delta S°}{R} - \frac{\Delta H°}{RT} \qquad (9)$$

where K_d is the distribution coefficient, R is the universal gas constant (8.314 J mol^{-1} K^{-1}), T is the temperature in Kelvin, $\Delta S°$ is standard entropy, and $\Delta H°$ is standard enthalpy.

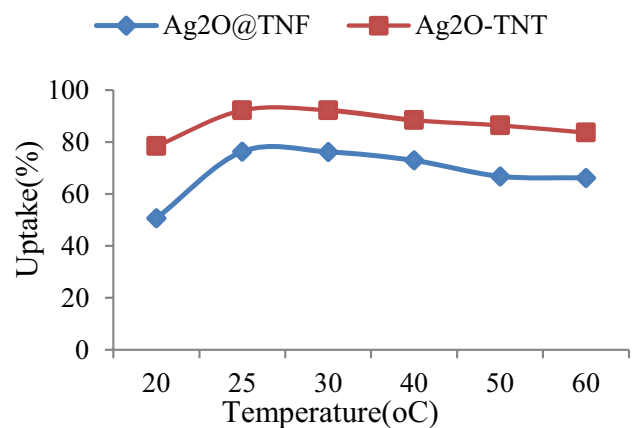The standard free energy change ($\Delta G°$) can be calculated from the Eq. (10):

Fig. 10 Effect of temperature on the absorption of I^- ions by $Ag_2O@TNT$ and $Ag_2O@TNF$ powder

Adsorbents type	Maximum adsorption capacity(mg/g)	pH range	BET surface area (m^2.g^{-1})	References
Ag_2O-T3NT	571.1	4–7	156.5	(Yang et al. 2011)
Ag_2O-TNL	431.5	7	143.8	(Bo et al. 2013)
Ag_2O-TNF	381	7	24.6	(Yang et al. 2011)
$Ag_2O@Mg (OH)_2$	380.7	6	78.19	(Chen et al. 2018)
$Ag°/Ag_2O$	326	6–7	–	(Yu et al. 2018)
Ag_2O-$Na_2Nb_2O_6·H_2O$	291.9	6–9	–	(Liu et al. 2015)
3D Ag_2O-Ag/TiO_2	208	–	153.7	(Liu et al. 2015)
2-$Ag_2O@MCM$-41	31.1	4–10	724.8	(Wenlin et al. 2022a)
5-$Ag_2O@MCM$-41	83.2	4–10	520.6	(Wenlin et al. 2022a)
12.5-$Ag_2O@MCM$-41	134.6	4–10	395.1	(Wenlin et al. 2022a)
Halloysite/ Ag_2O	57.7	7–8	73.8	(Wenlin et al. 2022b)
$Ag_2O@ChNF$ aerogels	304.8	–	179.71	(Runan et al. 2017)
$Ag_2O@TNT$	344.83	7–8	105.4	This Work
$Ag_2O@TNF$	277.77	7–8	80.5	This Work

Table 4 Comparison of the maximum I^- adsorption capacities, pH and BET of $Ag_2O@TNT$ and $Ag_2O@TNF$ and other Ag_2O-based adsorbent

$$\Delta G° = \Delta H° − T\Delta S° \qquad (10)$$

Thermodynamic parameters ($\Delta G°$, $\Delta H°$ and $\Delta S°$) were computed by using the linear plot of ln K_d vs 1/T for I$^-$ ions adsorption on Ag$_2$O@TNT and Ag$_2$O@TNF as shown in Fig. 11. The estimate values of thermodynamic parameters for the adsorption of I.$^-$ ions at different temperatures are presented in Table 5

The results of thermodynamic parameters show that $\Delta H°$ values are positive for Ag$_2$O@TNT and Ag$_2$O@TNF synthesized adsorbents, while $\Delta G°$ values are negative. This indicates that adsorption of iodine ions on the both synthesized adsorbents are endothermic and spontaneous, and this state makes the process stable.

As $\Delta G°$ values become increasingly negative with rising temperatures, it points to enhanced adsorption efficiency at elevated temperatures (Atta and Akl 2015; Liu et al. 2013a, b, c). As $\Delta G°$ values become increasingly negative with increasing temperature, it indicates an increase in adsorption efficiency at high temperatures (Atta and Akl 2015; Liu et al. 2013a, b, c). At 298.15 K, $\Delta G°$ values for Ag$_2$O@TNT and Ag$_2$O@TNF are − 1.153 and − 0.357 kJ mol^{-1}, respectively, it shows that the adsorption of I$^-$ ions on Ag$_2$O@TNT is more favorable than Ag$_2$O@TNF. However, the absolute values of ΔG for both adsorbents remain below 20 kJ mol^{-1}, indicating that the adsorption of I$^-$ ions on the adsorbents is mainly through physical adsorption (Yousefipour et al. 2023). The enhanced physical adsorption on the Ag$_2$O@TNT surface can be attributed to its superior specific surface area.

Conclusion

In this research, it has been tried to synthesize modified Ag$_2$O@TNTs and Ag$_2$O@TNF adsorbents with the ability to absorb more iodine ions by increasing the alkalinity and reducing the time. The experimental results of this research shows that Ag$_2$O@TNTs and Ag$_2$O@TNF synthesized by hydrothermal method can be an effective adsorbent for the adsorption of I$^-$ ions from aqueous solutions under optimized conditions of pH 7, contact time about 7 min, T 25 ± 1 °C and mass of adsorbents 0.05 g per 20 ml. The kinetic, isotherm and thermodynamic studies confirmed the experimental results. The sorption kinetic studies show that the best-fitting kinetic model describe the adsorption mechanism as a linear form of pseudo-second-order model with regression coefficient ($R^2 = 0.9991$ for Ag$_2$O@TNT and $R^2 = 0.9988$ for Ag$_2$O@TNF). Moreover, according to the isotherm experimental data, the best-fitting isometric model to describe the relationship between I$^-$ ions and Ag$_2$O@TNT and Ag$_2$O@TNF adsorbents is Langmuir model white regression correlation ($R^2 = 0.9935$ for Ag$_2$O@TNT and $R^2 = 0.9913$ for Ag$_2$O@TNF). These experimental data indicated the adsorption was monolayer for both synthesized adsorbents. The maximum uptake capacity of I$^-$ ions was found from the Langmuir model for I$^-$ ions was 344.83 (mg g^{-1}) and 277.77 (mg g^{-1}) at 298 K and removal rates of 83.4% and 78.8%, for Ag$_2$O@TNT and Ag$_2$O@TNF, respectively. The R_L value for Ag$_2$O@TNT is 0.67 and for Ag$_2$O@TNF is 0.65, which confirms the of favorability adsorption.
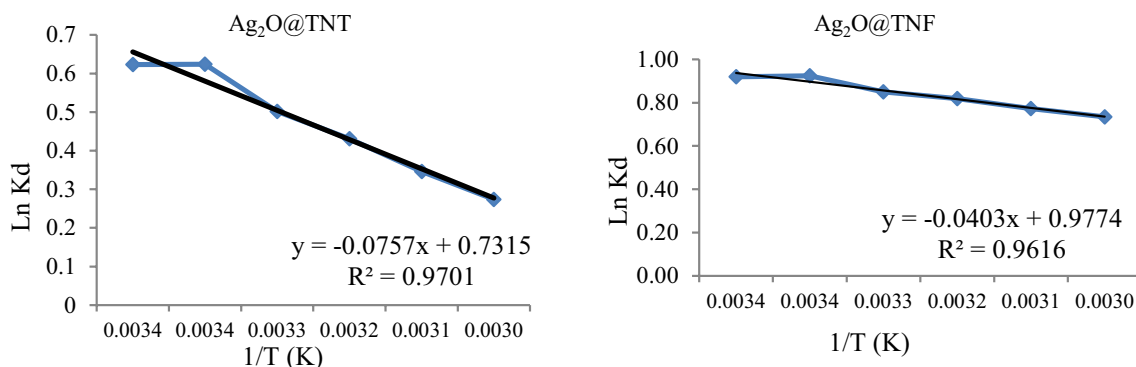

Fig. 11 Plot of $\ln K_L$ vs 1/T for determination of thermodynamic parameters for I$^-$ ions adsorption on Ag$_2$O@TNT and Ag$_2$O@TNF

Table 5 Thermodynamic parameters for I-ions on Ag$_2$O@TNT and Ag$_2$O@TNF

Sorbents	$\Delta H°$(kJ mol^{-1} k^{-1})	$\Delta S°$ (J mol^{-1} k^{-1})	$\Delta G°$(kJ mol^{-1})					
			293.15	298.15	303.15	313.15	323.15	333.15
Ag$_2$O@TNT	0.62937	0.0060	− 1.153	− 1.183	− 1.214	− 1.275	− 1.335	− 1.396
Ag$_2$O@TNF	0.335054	0.00812	− 0.357	− 0.369	− 0.381	− 0.405	− 0.428	− 0.452

Thermodynamic parameters show that the adsorption of I^- ions in the process of $Ag_2O@TNT$ and $Ag_2O@TNF$ is possible spontaneously and endothermically. Due to the large surface area of TNT and TNF, they acceptable ability to absorb Ag_2O, so I^- ion adsorption capacity on $Ag_2O@TNT$ and $Ag_2O@TNF$ is also high and fast.

Comparing the results of this work with similar projects indicates that I^- ions by synthesized $Ag_2O@TNT$ and $Ag_2O@TNF$ are fast and efficient adsorbents. These adsorbents can be easily synthesized and have a good ability in wastewater treatment. The tubular and fibrous structure of these adsorbents has made them easily separated from the wastewater after absorbing the ions treatment. Moreover, due to the strong chemical bond between Ag^+ and I^- ions and efficient physical placement of ions in $Ag_2O@TNT$ and $Ag_2O@TNF$ and no desorption, they have good stability for the safe disposal of radioactive iodine after the absorption process and are safe for the environment.

Author contributions **Taraneh Mostatabi:** Conceptualization, Methodology, Validation, Investigation, Formal analysis, Data curation, Writing—Original draft preparation **A. Nilchi.**: Supervision, Writing—Review & Editing, Project administration. **A. H. Hassani**: Visualization, Supervision, Review & Editing **S. Janitabar Darzi:** Methodology, Validation, Investigation, Writing—Review & Editing, Supervision.

Declarations

Conflict of interest The data included in this manuscript have yet to be published previously. All authors declare that they have no confict of interest.

References

Almarbd ZZ, Abbass NM (2022) Synthesis and characterization of TiO_2, Ag_2O, and graphene oxide nanoparticles with polystyrene as a nonocomposites and some of their applications. Eurasian Chem Commun 4:1033–1043

Abbasizadeh S, Saeed AR, Mousavian MA (2013) Preparation of a novel electrospun polyvinyl alcohol/titanium oxide nanofiber adsorbent modified with mercapto groups for uranium (VI) and thorium (IV) removal from aqueous solution. Chem Eng J 220:161–171

Atta AM, Akl ZF (2015) Removal of thorium from water using modified magnetite nanoparticles capped with rosin amidoxime. Mater Chem Phys 163:253–261

Bo A et al (2013) Removal of radioactive iodine from water using Ag_2O grafted titanate nanolamina as efficient adsorbent. J Hazard Mater 246:199–205

Chao D et al (2020) Comparison of Ag and Agi-modified zno as heterogeneous photocatalysts for simulated sunlight driven photodegradation of metronidazole. Catalysts 10:1097

Cheng H et al (2013) Tailoring AgI nanoparticles for the assembly of AgI/BiOI hierarchical hybrids with size-dependent photocatalytic activities. J Mater Chem A 1:7131–7136

Chen Y-Y et al (2018) One-step synthesis of $Ag_2O@Mg(OH)_2$ nanocomposite as an efficient scavenger for iodine and uranium. J Colloid Interface Sci 510:280–291

Chmielewská-Horváthová E, Lesnỳ J (1995) Iodide adsorption on the surface of chemically pretreated clinoptilolite. J Radioanal Nucl Chem 200:351–363

Dada AO, Olalekan AP, Olatunya AM, Dada OJIJC (2012) Langmuir, Freundlich, Temkin and Dubinin-Radushkevich isotherms studies of equilibrium sorption of Zn^{2+} unto phosphoric acid modified rice husk. IOSR J Appl Chem 3:38–45

Davit P, Martra G, C OLUCCIA, S., (2004) Photocatalytic degradation of organic compounds on TiO_2 powders, FT-IR investigation of surface reactivity and mechanistic aspect. J Jpn Petrol Inst 47:359–376

Decamp C, Happel S (2013) Utilization of a mixed-bed column for the removal of iodine from radioactive process waste solutions. J Radioanal Nucl Chem 298:763–767

ElShorafa R, Zhaoyang L, Said A (2023) Durable nanofiber-based membrane with efficient and consistent performance for oil/salt-water separation. Appl Sci 13(11):6792

Emadzadeh D et al (2015) Synthesis, modification and optimization of titanate nanotubes-polyamide thin film nanocomposite (TFN) membrane for forward osmosis (FO) application. Chem Eng J 281:243–251

Emran KM, Alsahli RMA (2021) Electrocatalytic hydrogen generation using sn loaded TiO_2 nanotubes. Int J Electrochem Sci 16:21068

Erhayem M et al (2015) Isotherm, kinetic and thermodynamic studies for the sorption of mercury (II) onto activated carbon from Rosmarinus officinalis leaves. Am J Anal Chem 6:1

Filipowicz B, Pruszynski M, Krajewski S, Bilewicz A (2014) Adsorption of ^{137}Cs on titanate nanostructures. J Radioanal Nucl Chem 301:889–895

GallardoáAmores JM, SanchezáEscribano V et al (1994) FT Raman and FTIR studies of titanias and metatitanate powders. J Chem Soc, Faraday Trans 90:3181–3190

Gao R, Lu Y, Xiao S, Li J (2017) Facile fabrication of nanofibrillated Chitin/Ag_2O heterostructured aerogels with high iodine capture efficiency. Sci Rep 7:4303

Ho Y-S, McKay G (1998) Sorption of dye from aqueous solution by peat. Chem Eng J 70:115–124

Ho Y-S, McKay G (1999) Pseudo-second order model for sorption processes. Process Biochem 34:451–465

Hsin-Hung O, Shang-Lien S-L (2007) Review of titania nanotubes synthesized via the hydrothermal treatment: fabrication, modification, and application. Sep Purif Technol 58:179–191

Ikari M et al (2015) Removal of iodide from water by chlorination and subsequent adsorption on powdered activated carbon. Water Res 68:227–237

Ikeda Y et al (1994) Adsorption of I ions on cinnabar for ^{129}I waste management. Radiochim Acta 65:195–198

Khan N, Burkitbayev M, Urakaev F (2019) Preparation and properties of nanocomposites in the systems S-AgI and S-Ag_2S-AgI in Dimethyl Sulfoxide. IOP Conf Ser: Mater Sci Eng 704(1):012007

Korobeinyk AV, Satayeva AR, Chinakulova AN, Inglezakis VJ (2018) Iodide removal by use of Ag-modified natural zeolites. s.l., s.n., p. 012014

Kowanga KD, Gatebe E, Mauti GO, Mauti EM (2016) Kinetic, sorption isotherms, pseudo-first-order model and pseudo-second-order model studies of Cu (II) and Pb (II) using defatted Moringa oleifera seed powder. The J Phytopharm 5:71–78

Lefevre G, Alnot M, Ehrhardt JJ, Bessiere J (1999) Uptake of iodide by a mixture of metallic copper and cupric compounds. Environ Sci Technol 33:1732–1737

Lefèvre G, Bessière J, Ehrhardt J-J, Walcarius A (2003) Immobilization of iodide on copper (I) sulfide minerals. J Environ Radioact 70:73–83

Lefèvre G, Walcarius A, Ehrhardt J-J, Bessière J (2000) Sorption of iodide on cuprite (Cu_2O). Langmuir 16:4519–4527

Li N et al (2012) Highly efficient, irreversible and selective ion exchange property of layered titanate nanostructures. Adv Func Mater 22:835–841

Liu J, Luo M, Yuan Z, Ping A (2013a) Synthesis, characterization, and application of titanate nanotubes for Th (IV) adsorption. J Radioanal Nucl Chem 298:1427–1434

Liu J, Mingbiao L, Yuan Z, Ping A (2013b) Synthesis, characterization, and application of titanate nanotubes for Th(IV) adsorption. J Radioanal Nucl Chem 298:1427–1434

Liu S et al (2015) Efficient removal of radioactive iodide ions from water by three-dimensional $Ag_2O–Ag/TiO_2$ composites under visible light irradiation. J Hazard Mater 284:171–181

Liu W, Sun W, Borthwick AGL, Ni J (2013c) Comparison on aggregation and sedimentation of titanium dioxide, titanate nanotubes and titanate nanotubes-TiO_2: Influence of pH, ionic strength and natural organic matter. Physicochem Eng Asp 434:319–328

Mao P et al (2017) Synthesis of Cu/Cu_2O hydrides for enhanced removal of iodide from water. J Hazard Mater 328:21–28

Morad I, El-Desoky MM, Mansour A, Wasfy M (2020) Synthesis, structural and electrical properties of PVA/TiO_2 nanocomposite films with different TiO_2 phases prepared by sol-gel technique. Journal of Materials Science Materials in Electronics, 27

Mostata, m., Ramadan, H. & EL. Amir, M., (2015) Sorption and desorption studies of radioiodine onto silver chloride via batch equilibration with its aqueous media. J Environ Radioact 150:9–19

Mu W et al (2016) Safe disposal of radioactive iodide ions from solutions by Ag_2O grafted sodium niobate nanofibers. Dalton Trans 45:753–759

Mu W et al (2017) Niobate nanofibers for simultaneous adsorptive removal of radioactive strontium and iodine from aqueous solution. J Alloy Compd 693:550–557

Nguyen N et al (2012) Simultaneous recovery of gold and iodine from the waste rinse water of the semiconductor industry using activated carbon. Mater Trans 53:760–765

Nhat HN, Hsunling B (2015) Effect of washing pH on the properties of titanate nanotubes and its activity for photocatalytic oxidation of NO and NO_2. Appl Surf Sci 355:672–680

Okada K et al (2015) Macroporous titanate nanotube/TiO_2 monolith for fast and large-capacity cation exchange. Chem Mater 27:1885–1891

Peng G-W, Chen S-K, Liu H-S (1995) Infrared absorption spectra and their correlation with the Ti-O bond length variations for TiO_2 (Rutile), Na-Titanates, and Na-Titanosilicate (Natisite, $Na_2TiOSiO_4$). Appl Spectrosc 49:1646–1651

Piccin JS, Dotto GL, Pinto LAA (2011) Adsorption isotherms and thermochemical data of FD&C Red n 40 binding by chitosan. Braz J Chem Eng 28:295–304

Reghunath S, Pinheiro D, KR S (2021) A review of hierarchical nanostructures of TiO_2: advances and applications. Appl Surf Sci Adv 3:2666–5239

Rodrigues CM, Ferreira OP, Alves OL (2010) Interaction of sodium titanate nanotubes with organic acids and base: chemical, structural and morphological stabilities. J Braz Chem Soc 21:1341–1348

Runan G, Yun GL, Shaoliang X, Jian L (2017) Facile fabrication of nanofibrillated Chitin/Ag_2O heterostructured aerogels. Sci Rep. 1

Sarina S et al (2014) Separate or simultaneous removal of radioactive cations and anions from water by layered sodium vanadate-based sorbents. Chem Mater 26:4788–4795

Sheng G et al (2012) Adsorption of Eu (III) on titanate nanotubes studied by a combination of batch and EXAFS technique. Sci China Chem 55:182–194

Sun H et al (2015) Modification of TiO_2 nanotubes by WO_3 species for improving their photocatalytic activity. Appl Surf Sci 343:181–187

Tatarchuk T, Shyichuk A, Mironyuk I, Naushad M (2019) A review on removal of uranium(VI) ions using titanium dioxide based sorbents. J Mol Liq 293:111563

Tri Yunarti R et al (2021) Study of Ag_2O/TiO_2 nanowires synthesis and characterization for heterogeneous reduction reaction catalysis of 4-nitrophenol. Nano-Struct & Nano-Objects 26:100719

Tsai C-C, Teng H (2006) Structural features of nanotubes synthesized from NaOH treatment on TiO_2 with different post-treatments. Chem Mater 18:367–373

Villavicencio M et al (2020) Ibuprofen photodegradation by Ag_2O and Ag/Ag_2O composites under simulated visible light irradiation. Catal Lett 150:2385–2399

Wang J et al (2022) Efficient capture of radioactive iodine by Ag-attached silica gel and its kinetics. Nucl Mater Energy 33:101270

Wenlin Y et al (2022a) Preparation of Halloysite/Ag_2O Nanomaterials and Their Performance for Iodide Adsorption. Minerals 12(3):304

Wenlin Y et al (2022b) Facile preparation of MCM-41/Ag_2O nanomaterials with high iodide-removal efficiency. Nanomaterials 12(20):3678

Xu J et al (2012) Hydrothermal synthesis and characterisation of potassium/sodium titanate nanofibres at different temperatures. Micro & Nano Letters, IET 7:654–657

Yang DJ et al (2008) Titanate nanofibers as intelligent absorbents for the removal of radioactive ions from water. Adv Mater 20:2777–2781

Yang D et al (2013a) Silver oxide nanocrystals anchored on titanate nanotubes and nanofibers: promising candidates for entrapment of radioactive iodine anions. Nanoscale 5:11011–11018

Yang D et al (2013b) Titanate-based adsorbents for radioactive ions entrapment from water. Nanoscale 5:2232–2242

Yang D et al (2011) Capture of radioactive cesium and iodide ions from water by using titanate nanofibers and nanotubes. Angew Chem Int Ed 50:10594–10598

Yang L et al (2016) Removal of radioactive iodide from simulated liquid waste in an integrated precipitation reactor and membrane separator (PR–MS) system. Sep Purif Technol 171:221–228

Yong NL, Ahmad A, Mohammad AW (2013) Synthesis and characterization of silver oxide nanoparticles by a novel method. Int J Sci Eng Res. 4

Yousefipour K, Janitabar Darzi S, Iravani E (2023) Schiff base-functionalized mesoporous titania: an efficient sorbent for the removal of radioactive thorium ions from aqueous solution. J Radioanal Nucl Chem 332:2447–2458

Yuan, et al (2016) Computational screening of iodine uptake in zeolitic imidazolate frameworks in a water-containing system. Phys Chem Chem Phys 18:23246–23256

Yu F et al (2018) Enhanced removal of iodide from aqueous solution by ozonation and subsequent adsorption on $Ag-Ag_2O$ modified on Carbon Spheres. Appl Surf Sci 427:753–762

Zhang H et al (2012) Iodide adsorption onto three organic–inorganic composite adsorbents. Adsorpt Sci Technol 30:449–460

Zhang X, Gu P, Li X, Zhang G (2017) Efficient adsorption of radioactive iodide ion from simulated wastewater by nano Cu_2O/Cu modified activated carbon. Chem Eng J 322:129–139

Zhang Y et al (2015) Titanate and Titania nanostructured materials for environmental and energy applications: a review. RSC Adv 5:79479–79510

Zia MR et al (2021) Removal of radioactive iodine using silver/iron oxide composite nanoadsorbents. Nanomaterials 11:588

Zima TM, Baklanova NI, Utkin AV (2012) Hydrothermal synthesis of a nanostructured TiO$_2$-based material in the presence of chitosan. Inorg Mater 48:821–826